Characteristics of Elongated Vapour Cloud Explosions

Jihui Geng, Baker Engineering and Risk Consultants, 3330 Oakwell Court, Suite 100, San Antonio, TX 78218-3024
Kelly Thomas, Baker Engineering and Risk Consultants, 3330 Oakwell Court, Suite 100, San Antonio, TX 78218-3024
Quentin Baker, Baker Engineering and Risk Consultants, 3330 Oakwell Court, Suite 100, San Antonio, TX 78218-3024

The purpose of this paper is to characterize elongated vapour cloud explosions (VCEs) and to identify the resultant difference in blast wave shape relative to those predicted by well-known VCE blast prediction methodologies (e.g., BST, TNO, etc.), the blast curves for which are normally based on an assumption that the flammable gas cloud is hemispherical and located at grade level. BakerRisk's Blast Wave Target Interaction (BWTI™) computational fluid dynamics (CFD) code was used to investigate the VCE blast loads resulting from elongated flammable gas clouds. The BWTI™ predictions were first validated against the recent Buncefield JIP test data. A blast wave diagram was developed to illustrate typical blast waves generated during the initial flame acceleration process and the subsequent flame propagation. It was found that the aspect ratio of the elongated cloud/congestion volume (i.e., ratio of length to width to height) has a significant impact on the resultant blast wave shape. The blast wave shape in elongated VCEs is was found to be controlled by the negative phase, which is generated by the primary blast wave during the initial acceleration phase in which an effective spherical (or cylindrical) flame front still exists. This primary negative phase plays a key role in the follow-on flame acceleration process, which either attains a steady flame speed or experiences a deflagration-to-detonation transition (DDT).

Keywords: vapor cloud explosion, elongated cloud, blast wave shape, CFD

Introduction

There have been several recent accidental vapour cloud explosions (e.g., Buncefield, UK 2005 and Jaipur, India 2009) which generated blast loads at the edge of cloud where some degree of congestion was present. In particular, the blast loads from the Buncefield incident were reported to show overpressures up to about 2 barg at the cloud/congestion edge, which then diminished rapidly with distance. It was concluded that the trees and undergrowth along a plant boundary on the Buncefield site, which formed an elongated congested volume, caused flame acceleration up to a velocity of several hundred m/s. This elongated congestion played a key role in the flame acceleration, resulting blast loads and subsequent observed structural damage.

Blast waves from explosion sources like a vapour cloud explosion (VCE), pressure vessel burst or high explosive exhibit both positive and negative phases, and the relative magnitude of the positive and negative phases varies among these types of explosion sources and the specific source characteristics. VCEs can be categorized into two modes, deflagrations and detonations, according to propagation mechanisms. In a vapor cloud deflagration, the flame propagates through the unburned fuel-air mixture at a flame velocity less than the speed of sound in the reactant gas mixture, while a detonation propagates at supersonic velocity. The blast curves for simplified VCE blast load prediction methodologies are normally based on an assumption that the flammable gas cloud is hemispherical and located at grade level (CCPS 2010). Numerous studies (e.g., Strehlow et al., 1979, Baker et al., 1983, van de Berg, 1985, Lenoir and Davenport, 1992) have shown that as the flame speed increases, the rate of pressure rise and the peak blast overpressure both increase. VCE blast waves can be characterized in three regimes: acoustic wave, pressure wave and shock wave (Tang and Baker, 1999). These blast wave regimes can be overlaid on Baker-Strehlow-Tang (BST) scaled overpressure curves (Geng and Baker, 2014). The bounds of regimes in flame speed M_f are approximately:

a) Acoustic – less than Mach 0.35

b) Pressure wave – Mach 0.35 to Mach 1.0

c) Shock wave – greater than 1.0

Elongated congestion patterns are commonly seen on most chemical processing facilities. However, there are few research evaluations reported for elongated VCEs (Pickles and Bittleston, 1983) and the blast loads from the elongated VCEs have not been fully addressed in VCE prediction methods. The purpose of this paper is to characterize elongated vapour cloud explosions (VCEs) and to identify the resultant difference in blast wave shape relative to those predicted by well-known VCE blast prediction methodologies, the blast curves for which are based on an assumption that the flammable gas cloud is hemispherical and located at grade level.

BakerRisk's Blast Wave Target Interaction (BWTI™) computational fluid dynamics (CFD) code (Thomas et al. 2006, Geng et al. 2007 and 2011) was used to investigate the VCE blast loads resulting from elongated flammable gas clouds. The BWTI™ predictions were first validated against the recent Buncefield JIP test data. A blast wave diagram was developed to illustrate typical waves generated during the flame acceleration process and their subsequent interaction.

Terminology for Elongated VCEs

Parameters for an elongated cloud

Figure 1 depicts an elongated flammable cloud with a length L, a width W and a height H. It assumed that the cloud covers a congested volume (i.e., that none of the cloud occupies an empty uncongested space), so that the cloud and the congested volume have the same dimensions. The following parameters are utilized to characterize the cloud geometry:

$$\textit{Free Vent Distance:} \qquad L_{FV} = MIN\left(H, \frac{w}{2}\right)$$

$$\textit{Cylindrical Distance:} \qquad L_{Cyl} = MAX\left(H, \frac{w}{2}\right)$$

$$\textit{Equivalent Radius of Cross Section:} \qquad R_{Equiv} = \sqrt{\frac{2 \cdot H \cdot W}{\pi}}$$

The cylindrical distance is introduced to measure the maximum distance a cylindrical flame front can travel before reaching the edge of the cloud. For the purposes of this paper, a flammable cloud is considered to be "elongated" if the ratio of the cloud length to the free vent distance (L / L_{FV}) is larger than 10 and the ratio of the cylindrical distance to the free vent distance (L_{Cyl} / L_{FV}) does not exceed 2. That is, a cloud is considered to be elongated if:

$$MAX\left(H, \frac{w}{2}\right) \le 2 \cdot MIN\left(H, \frac{w}{2}\right), \text{ and}$$

$$L > 10 \cdot MIN\left(H, \frac{w}{2}\right)$$

The elongated cloud is characterized by two parameters: (1) the aspect ratio (*L/W/H*) and (2) a characteristic distance represented by either the free vent distance (L_{FV}) or the equivalent radius (R_{Equiv}). The three cloud parameter sets specifically evaluated in this work are given in Table 1. The "Example Case" cloud is a parametric example case, whereas the "Buncefield" and "BakerRisk" clouds correspond to test rigs. The "Example Case" cloud listed in Table 1 has dimensions of L=37 m, W=7.32 m and H=1.83 m and has (1) an aspect ratio of 20/4/1 and (2) a free vent distance (L_{FV}) of 1.83 m and an equivalent radius (R_{Equiv}) of 2.92 m (along with a cylindrical distance of 3.66 m). This cloud is referred to as "20/4/1 – 1.83 m" or "20/4/1 – R 2.92 m" within the context of this paper. The BakerRisk test rig has dimensions of L=22 m (72 ft), W=3.66 m (12 ft) and H=1.83 m (6 ft) is referred to as "12/2/1 – 1.83 m" or "12/2/1 – R 2.06 m". The Buncefield JIP Test #6 configuration has dimensions of L=45 m, W=4.5 m and H=3 m is referred to as "15/1.5/1 – 2.25 m" or "15/1.5/1 – R 2.93 m".
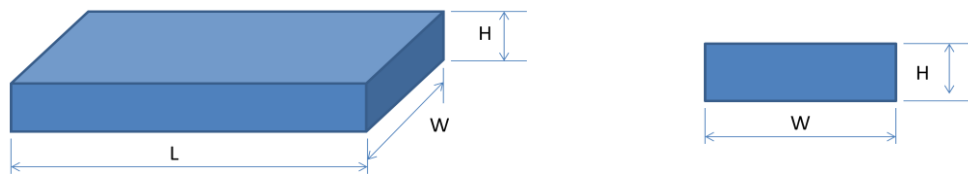

Figure 1. Dimensions of Elongated Vapour Cloud (L / L_{FV} >10)

Table 1. Characteristic Parameters of Elongated Vapour Cloud

Test Rig	Cloud in Congestion								Volume
	Dimensions [m]						Aspect Ratio		
	Length L	Width W	Height H	L_FV	L_Cyl	R_Equiv	L/W/H - L_FV	L/W/H - R_Equiv	[m³]
Example Case	37	7.32	1.83	1.83	3.66	2.92	20/4/1 - 1.83 m	20/4/1 - R 2.92 m	490
BakerRisk (12x2x1)	22.0	3.66	1.83	1.83	1.83	2.06	12/2/1 - 1.83 m	12/2/1 - R 2.06 m	147
Buncefield JIP (Test3.2 #6)	45	4.5	3	2.25	3	2.93	15/1.5/1 - 2.25 m	15/1.5/1 - R 2.93 m	608

Characteristic parameters for elongated VCEs

The blast field generated by an elongated cloud depends on several characteristic parameters, as discussed in the following sections. The three characteristic parameters examined in this work are as follows:

1) Characteristic time (t_n), which is defined as the time for a rarefaction wave to travel from the cloud edge to the cloud center or ignition location.

2) Energy release rate (dV/dr), which is expressed in terms of the volume of flammable gas cloud consumed per unit flame travel distance (V is volume and r is the flame front position).

3) Radial expansion factor (F_{Exp}), which is defined in terms of the expansion of unburned gas ahead of the flame front.

The characteristic time (t_n) is defined by:

$$t_n = \frac{R_{Eq}}{C}$$

where C is the ambient sound speed (taken to be that for air, 334 m/s = 1.1 ft/ms).

Characterizing the energy release rate as dV/dR assumes a constant energy density in the cloud, which is correct of the test cases evaluated here. This parameter is expressed differently depending on the location of the flame front within the cloud. Consider, for example, the case of the "General" cloud ("20/4/1 – 1.83m") with ignition at the cloud center. **Figure 2** shows fourdifferent flame front positions and corresponding times; expansion and distortion of the cloud due to the passage of the flame front is not reflected in this figure for the sake of simplicity. At time t_1 the flame reaches the top of cloud (i.e., r = L_{FV}), the flame is spherical, and the energy release rate up to this time is:

$$dV/dr_{r<L\_FV} = 2\pi r^2$$

Between t_1 and t_2 the flame travels to the side of the cloud/congestion (i.e., at t_2, r = L_{Cyl}), at which point the flame front shape is neither spherical nor cylindrical. The energy release rate during this time period (t_1 to t_2) can be approximated as:

$$dV/dr_{L_{FV}<r<L_{Cyl}} = 2\pi L_{FV} r$$

Time t_4 is defined as that time at which the flame front reaches $2L_{Cyl}$, and there after the flame front is almost planar and the energy release rate can be expressed as:

$$dV/dr_{r>2L_{Cyl}} = LW$$

Between t_2 and t_4, the energy release rate can be approximately linearized from a rate of $2\pi L_{\_FV} r$ to LW.

The radial expansion factor (F_{Exp}) is a function of flame speed, with a lower flame speed giving a higher expansion factor. The volume expansion factor due to gaseous hydrocarbon fuel combustion is around 8 for a stoichiometric mixture with air, which gives a radial expansion factor of between 1 and 2, depending on flame speed.

Figure 3 provides an example of a normalized energy release rate distribution along the long-axis of the cloud, both without and with cloud expansion taken into account, as shown in top and bottom charts, respectively. The energy release rates were normalized by *LW,* the cloud cross sectional area, so that the energy release rate is unity at long flame travel distances. The flame travel distance was normalized by the free vent distance (L_{FV}), so that the total cloud length would be approximately 20 (i.e., 37/1.83 = 20.2) and the half-length of the cloud would be approximately 10. A radial expansion factor (F_{Exp}) of 1.5 was used for illustrative purposes. The normalized energy release rate distribution without cloud expansion (top chart) matches the schematic description shown in Figure 2. However, the normalized energy release rate distribution with cloud expansion (bottom chart) better explains the blast field resulting from an elongated VCE, as discussed in the following numerical modelling example.
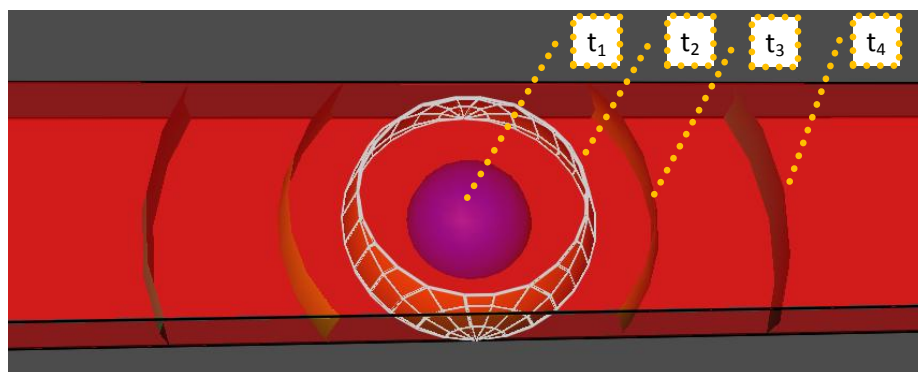

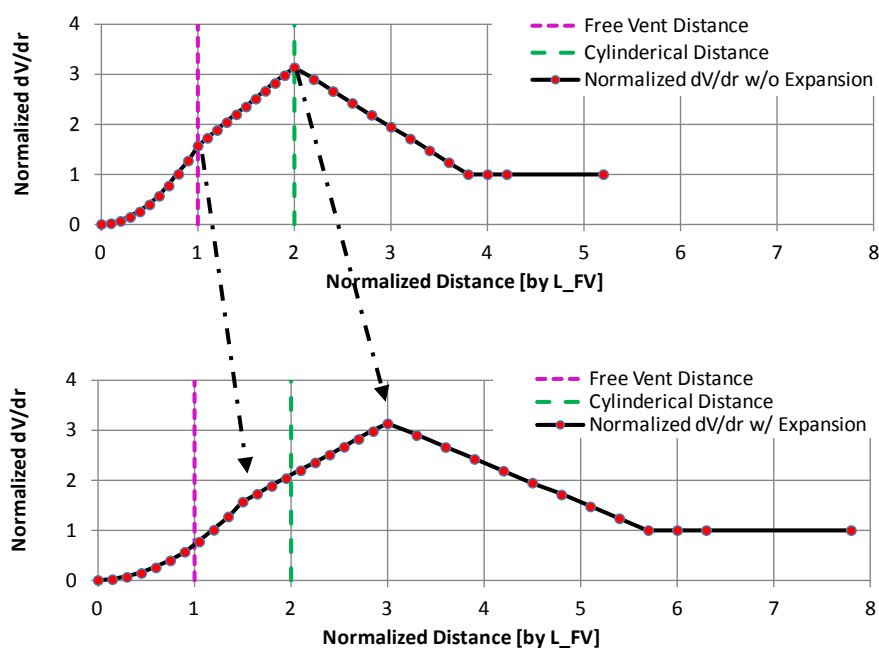**Figure 2. Schematic Description of Flame Shape in Elongated Cloud (20/4/1 -1.83 m Cloud)**

Figure 3. Energy Release Rate Distribution without (top) and with (bottom) Cloud Expansion (20/4/1 - 1.83 m Cloud)

Example of Elongated VCEs

A VCE of the "Example Case" cloud (20/4/1 – 1.83 m) configuration, shown in Figure 2 & Figure 3, was numerically modelled using the FLACS CFD code to illustrate the resulting flammable cloud expansion and blast field. Figure 4 shows the fuel concentration (ER: equivalence ratio) and overpressure contours at selected times. Only half (i.e., the "right half") of the domain is shown in these figures since the cloud was ignited at the bottom center of the cloud. The fuel ER and pressure scales shown in these figures are from LFL (lower flammable limit) to 1.0 (stoichiometric ER) and from 0.007 barg (0.1 psig) to 0.1 barg (1.5 psig), respectively. The fuel concentration contours are shown to illustrate both the flame front development and the resultant expansion of the unburned fuel cloud. Both elevation (side) and plan (top) views of the fuel concentration contours are provided. The distance scale is normalized distance by the free vent distance L_{FV} (equal to the height of the cloud for the case), so that the cloud half-length is approximately 10 (i.e., only the central portion of the cloud is shown in the fuel concentration contours).

As the flame reaches the initial height of the cloud (i.e., L_{FV}) at a normalized flame travel distance of 1 and at a time of about 0.26 seconds, the cloud has expanded significantly in the vertical direction near the cloud center, but the expansion along the horizontal direction is a relatively small percentage of the longitudinal length. The pressure continues to build up near the central part of cloud until about 0.26 s (see Figure 4). As the accelerating flame arrives at the normalized distance of 2 (at around 0.29 s), it reaches the sides of the cloud, and the period during which the flame can be characterized as cylindrical ends. A group of rarefaction waves begin traveling inward from the sides as a result, and this continues until a time of about 0.33 s when the leading flame front reaches a normalized distance of about 4. During this process, the high pressure core moves longitudinally down congestion with the flame front while a negative phase develops in the central portion of the cloud. After 0.33 s, the high pressure core retains the same basic pattern as the flame travels through the remainder of the cloud at a nearly constant flame speed, as can be seen in Figure 5, which illustrates the propagation through the remainder of the cloud. Times of 0.37 s and 0.41 s correspond to the flame arrival location at the normalized distances of 6 and 8, respectively.

The flame speed (Mach No.) distribution along the long-axis direction and overpressure histories at selected locations are given in Figure 6 and Figure 7, respectively. A simplified flame speed distribution is depicted in Figure 6, indicating three phases of the flame acceleration: (1) one during the time when the flame front is spherical, (2) a second when the flame front is cylindrical, and (3) the latter portion of the flame propagation, where the flame speed is approximately steady (constant) when the flame front is planar. These are illustrated in Figure 3. The three distinct energy release rates regimes can be characterized as: (1) L/L_{FV} from 0 to 1.5, where the flame front is spherical and the flame speed increases linearly, (2) L/L_{FV} from 1.5 to 3.0, where the flame front is cylindrical and the flame acceleration is reduced, indicating that the energy release by the cylindrical flame front provides a weaker source to support the 3D expansion, and (3) L/L_{FV} greater than 3, where the flame speed reaches approximately Mach 0.27. The drop in the energy release rate in the third regime, as illustrated in Figure 3, can only support a steady flame propagation (with some oscillations about the steady value). The primary pressure peak due to the initial flame acceleration decouples from the flame front as this 3rd regime is entered, which can be seen in the pressure histories at locations beyond $L/L_{FV} = 4$, leading to the double peak in the pressure-time history which can be seen in Figure 7.

The double peak pressure signal was also evident in BakerRisk's recent experiments performed with the "BakerRisk" cloud configuration (12/2/1 – 1.83 m, see Table 1). The maximum flame speed attained in the tests was $M_f = 0.4$. The first (or the primary) peak was much more pronounced than the one shown in Figure 7.
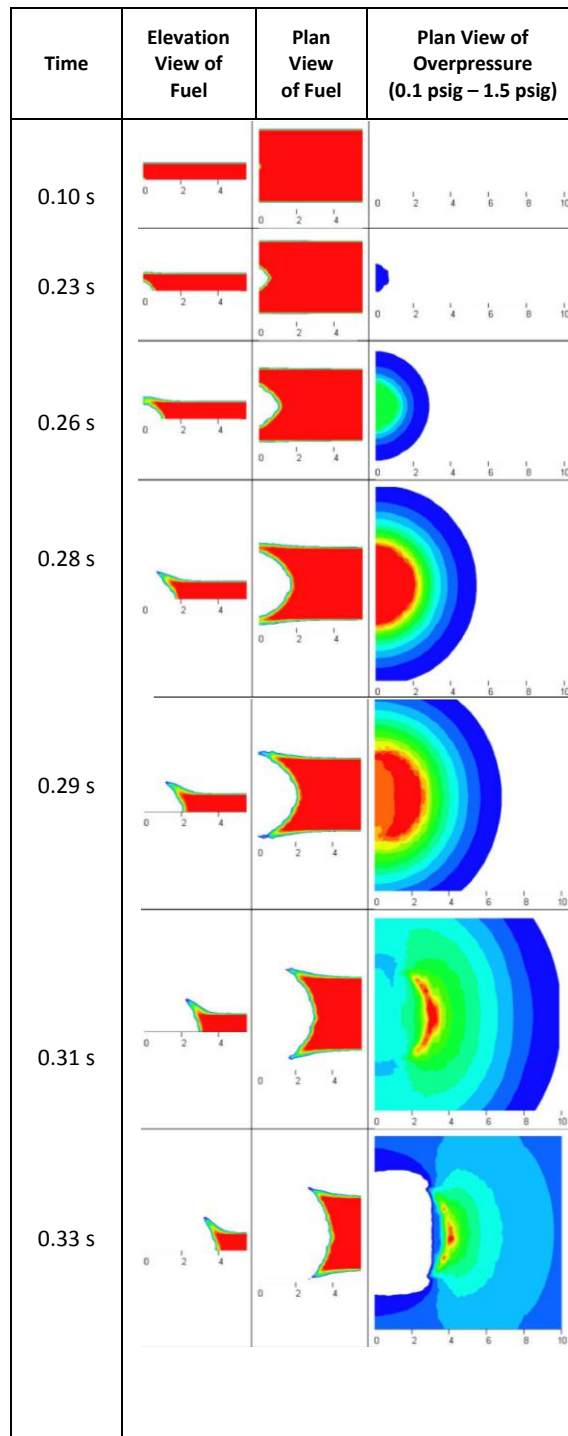

Figure 4. Typical Blast Field from an Elongated Vapour Cloud, Example Case (20/4/1 – 1.83 m Cloud, Ctr-Ign, 1 of 2)
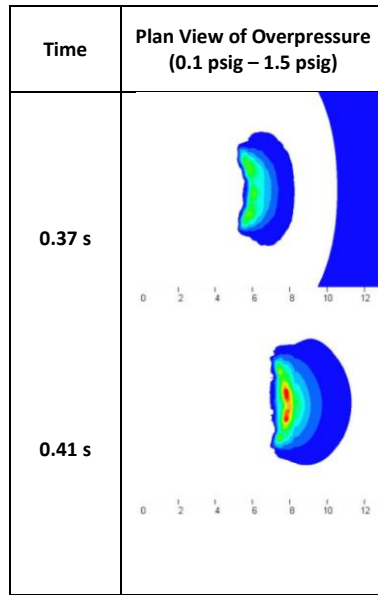
Time	Plan View of Overpressure (0.1 psig – 1.5 psig)
0.37 s	
0.41 s	

Figure 5. Overpressure Contours with Flame near Cloud End, Example Case (20/4/1 – 1.83 m Cloud, Ctr-Ign, 2 of 2)
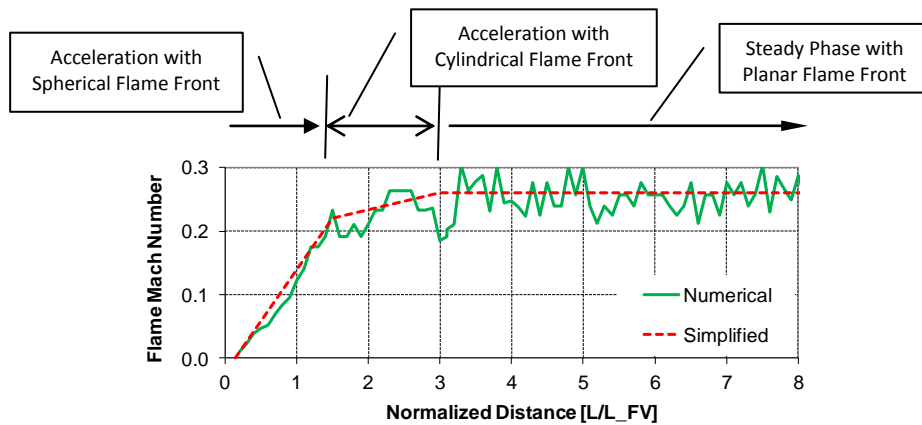

Figure 6. Flame Speed Distribution and Pressure Histories (20/4/1 – 1.83 m Cloud, Ctr-Ign)
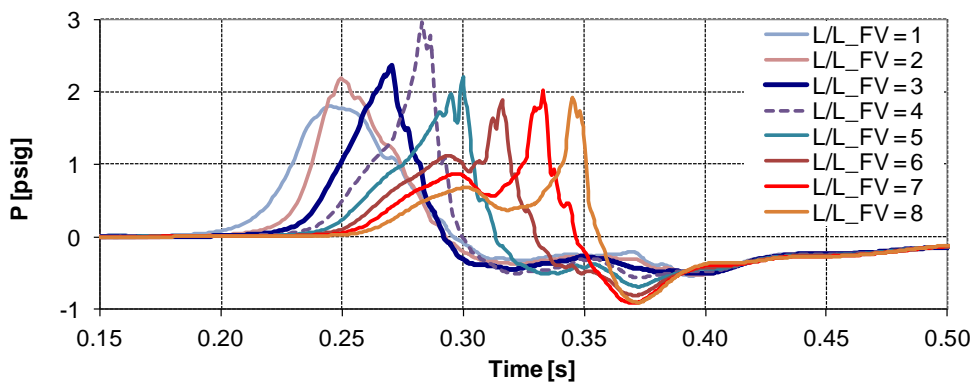

Figure 7. Pressure Histories (20/4/1 – 1.83 m Cloud, Ctr-Ign)

Validation against Buncefield JIP Test Data

Table 1 provides the elongated cloud configuration (15/1.5/1 − 2.25 m, 15/1.5/1 − R 2.93 m) for Test 3.2 #6 from the Buncefield JIP test program. The cloud, which covered a congested volume made up of vegetation, was 45 m long, 4.5 m wide and 3 m high. Ignition was at one end of the cloud, 1 m inside the cloud edge. The cloud length ratio (L/L_{FV}) is greater than 15. BakerRisk's BWTI™ CFD code was selected to model the blast loads, due to the large length ratio, with a prescribed flame speed that matched the measured flame speed, which ensured that the constant flame speed after the initial acceleration phase in the cloud was modelled reasonably. Figure 8 (a) shows the measured flame speed and the simplified flame speed distribution which used in the BWTI™ simulation. The flame speed increases linearly from 0 m/s at ignition location to 100 m/s at a distance of 6 m and then is constant at 100 m/s (Mach 0.3). Unlike the previous example where the characteristic distance ratio of $L_{Cyl}/L_{FV} = 2$ resulted in two phases of flame acceleration, the Buncefield JIP cloud has a L_{Cyl}/L_{FV} of 1.3 and produced a single flame acceleration phase.

Figure 8 (b) compares the BWTI prediction of overpressure with the Buncefield JIP measured data, showing reasonable agreement both inside and outside the congestion areas. Figure 9 compares the pressure histories at selected locations (6 m, 18 m, 30 m and 45 m). The blast wave shape predicted by BWTI is in reasonable agreement with the test data, including the double peaks. The agreement at the end of the cloud in particularly good for both the positive and negative overpressure. The flame speed attained with this cloud configuration is comparable to the one obtained in the example case (Figure 6).
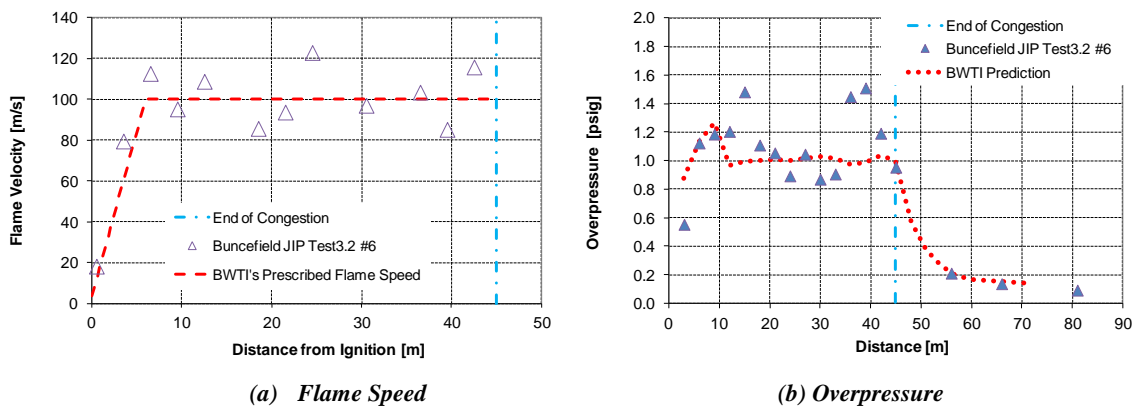

(a) Flame Speed   *(b) Overpressure*

Figure 8. Flame Speed and Pressure Distribution (Buncefield JIP Test 3.2-#6, V_f = 100 m/s)

6 m (L/L$_{FV}$ = 2.7)   *18 m (L/L$_{FV}$ = 8)*

30 m (L/L$_{FV}$ = 13.3)   *45 m (L/L$_{FV}$ = 20)*
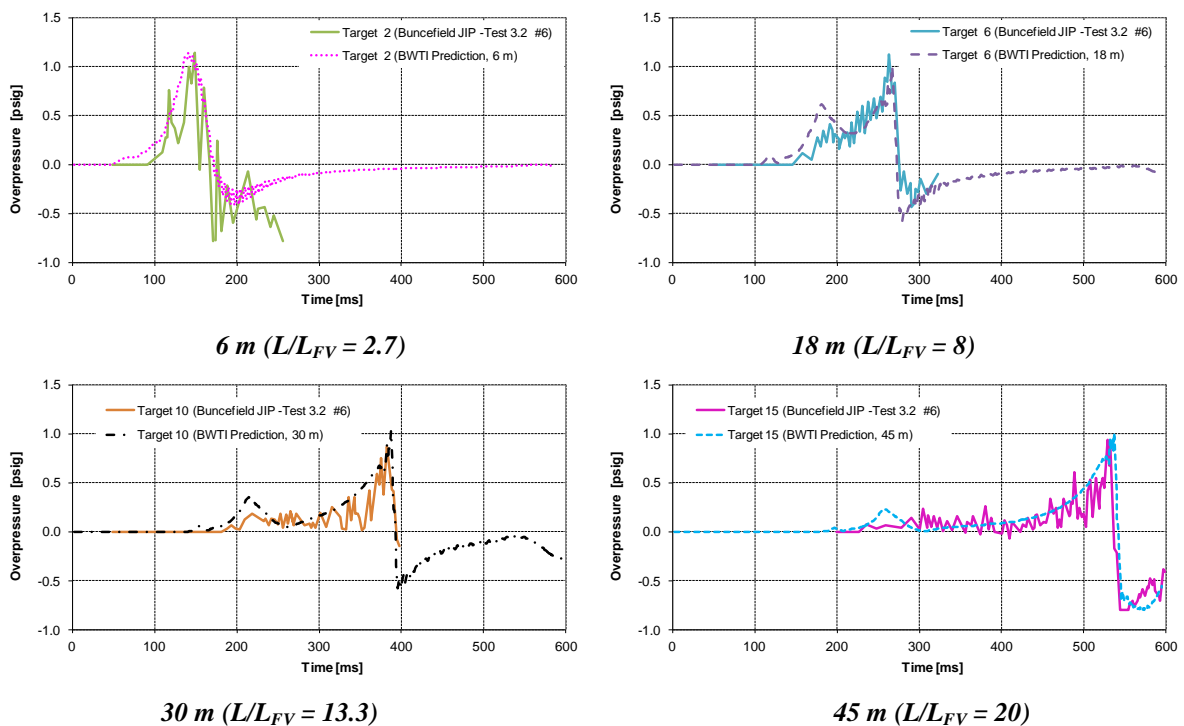
Figure 9. Pressure History Comparison with Buncefield JIP (Test 3.2-#6, V_f = 100 m/s)

Blast Wave Diagrams for Elongated VCEs

The same cloud configuration as the Buncefield Test 3.2 #6 (15/1.5/1 – 2.25 m or 15/1.5/1 – R 2.93 m) was employed to generate distance time (x-t) wave diagrams and associated pressure histories at selected locations in order to examine the impact of the flame speed on the resultant blast wave shape. The flame was assume to have a constant acceleration out to 6 m (L/L_{FV} = 2.7), at which point a constant velocity was employed. Constant flame velocities of 100 m/s, 200 m/s and 300 m/s were evaluated.

Flame speed of 100 m/s (Mach No: 0.3)

Figure 10 (a) shows a wave diagram for an accelerating flame with a final flame velocity of 100 m/s at a distance of 6 m (L/L_{FV} = 2.7). The distance in the horizontal axis is normalized by the free vent distance L_{FV} (2.3 m) and the time in the vertical axis is normalized by the characteristic time (t_n = 2.93 m / 334 m/s = 8.8 ms). The wave diagram includes trajectories for the accelerating flame, the leading acoustic wave (due to any disturbance), the primary pressure peak (due to the initial flame acceleration), the second pressure peak (due to the steady subsonic flame) and the start of the negative phase. The free vent distance (2.3 m), the cylindrical distance (3 m) and the flame acceleration distance (6 m) are also denoted in the figure.

The pressure histories at normalized distances (L/L_{FV}) of 4.0 and 5.8 and 7.6 are given in Figure 10 (b). As discussed previously, the slow speed of the steady flame allows the primary and second pressure waves to decouple beyond a distance (L/L_{FV}) of approximately 6, resulting in the first peak to rapidly decay while the second peak remains at about 1.0 psig.

Flame speed of 200 m/s (Mach No: 0.6)

Figure 11 (a) shows a wave diagram for an accelerating flame with a final flame velocity of 200 m/s. The pressure histories at normalized distances (L/L_{FV}) between 4.0 and 12.9 are given in Figure 11 (b). As can be seen by comparing Figure 11 and Figure 10, increasing the flame speed slows down the decoupling between the primary and second pressure peaks, while the second peak remains constant beyond an L/L_{FV} of approximately 10.

Flame speed of 300 m/s (Mach No: 0.9)

Figure 12 (a) shows a wave diagram for an accelerating flame with a final flame velocity of 300 m/s. The pressure histories at normalized distances (L/L_{FV}) between 4.0 and 14.7 are given in Figure 12 (b). The energy release rate for this case is sufficiently high that the burning of the postulated steady flame provides positive feedback to the primary blast wave, which therefore experiences a slower decay (i.e., as compared to the decay rate with lower flame speeds, see Figure 11 (b)). The peak pressure remains constant at about 10 psig beyond an L/L_{FV} of approximately 10.
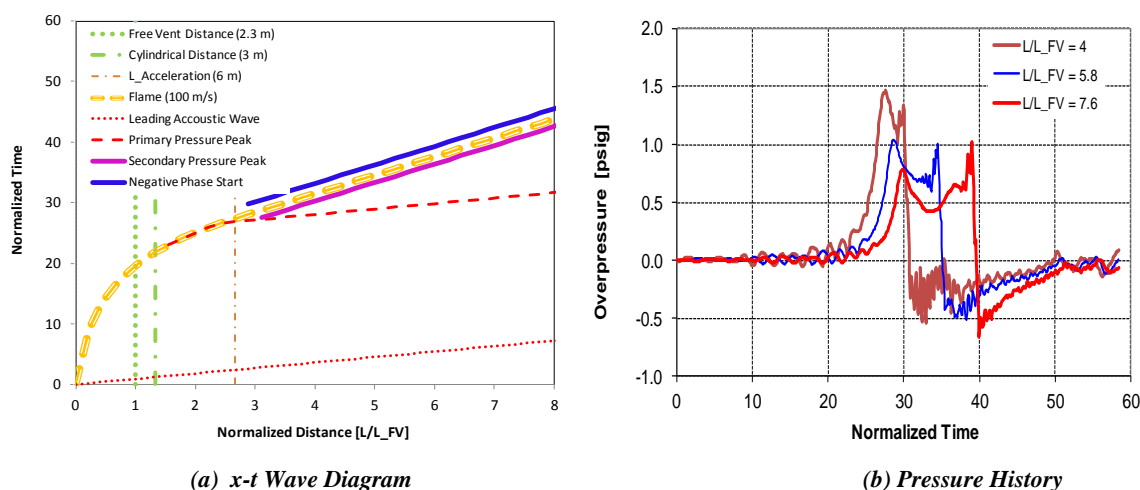

(a) x-t Wave Diagram   *(b) Pressure History*

Figure 10. Wave Diagram and Pressure Histories at Selected Locations for a Flame Velocity of 100 m/s

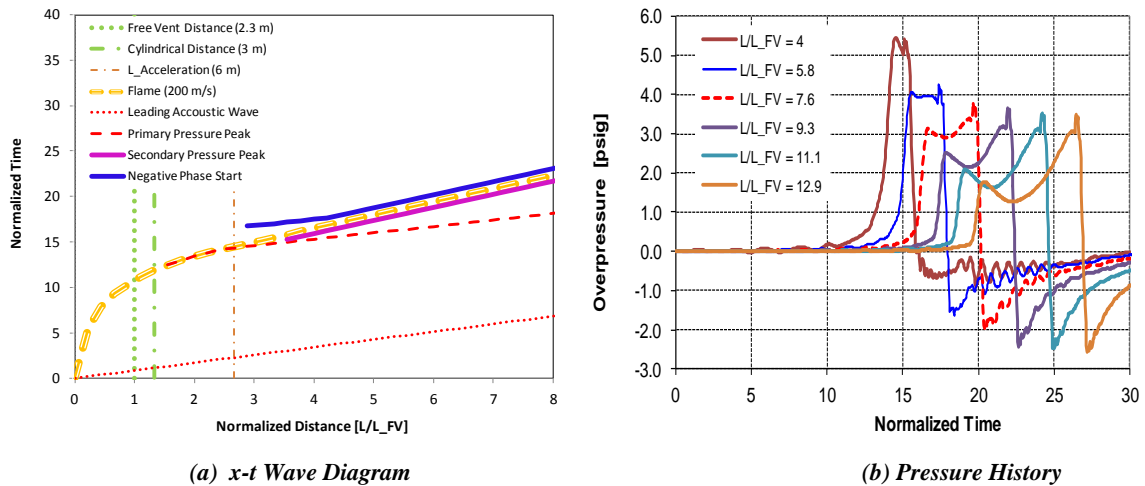*(a) x-t Wave Diagram*   *(b) Pressure History*

Figure 11. Wave Diagram and Pressure Histories at Selected Locations for a Flame Velocity of 200 m/s

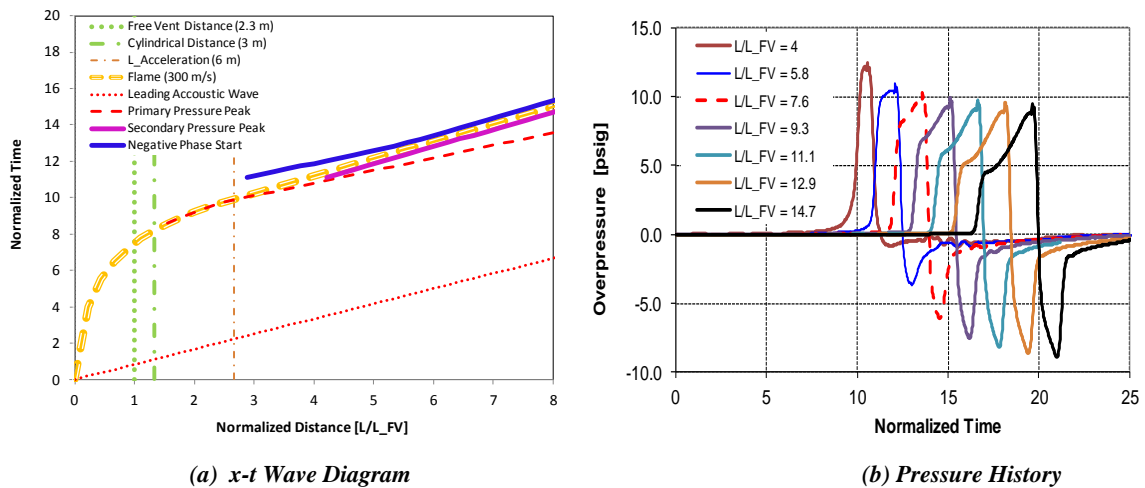*(a) x-t Wave Diagram*   *(b) Pressure History*

Figure 12. Wave Diagram and Pressure Histories at Selected Locations for a Flame Velocity of 300 m/s

Discussion

Near-field blast loads from elongated VCEs

Figure 13 shows the blast wave outside the cloud for flame speeds of Mach 0.6 and Mach 0.9. The standoff distance (D) is measured from the cloud end. The positive phase transition rapidly to a negative phase, with the peak negative pressure being comparable to, or even larger than, the peak positive pressure.

For a flame speed of Mach 0.9 (Figure 13 (b)), the pressure at the end of the cloud (D=0) drops from the peak positive pressure (9.0 psig) to the peak negative pressure (-10 psig) within the normalized characteristic time *(t_n* = 8.8 ms). The difference between the peak positive and negative pressure is 19 psig (1.3 barg). A comparable pressure drop occurs at a standoff distance of 6 m (D/L_{FV} = 2.7). The drop between the peak positive and negative pressures diminishes quickly with distance. This localized pressure drop is due to the high pressure core traveling with the flame front (i.e., in the region beyond an *L/L_{FV}* of 6) in an elongated VCE (see Figure 5).
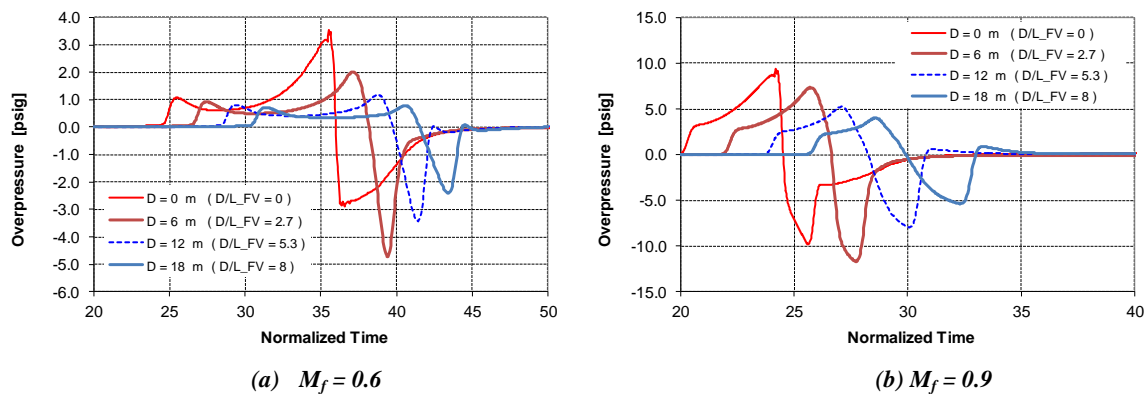
9

(a) $M_f = 0.6$ *(b)* $M_f = 0.9$

Figure 13. Pressure Histories at Selected Locations beyond Congestion End

Blast wave shape of elongated VCEs

As discussed previously, VCE blast waves can be characterized in three regimes: shock wave, pressure wave and acoustic wave. The blast wave shape for an elongated VCE resembles an acoustic wave, as can be seen be examining Figure 9 (M_f=0.3), Figure 11 (M_f = 0.6) and Figure 12 (M_f = 0.9). Of course, the magnitudes of the peak positive and negative phases are larger than with a traditional acoustic wave. This wave shape is the result of the isolated high pressure core associated with a steady flame speed propagating down the length of the cloud outside the initial explosion region (i.e., beyond an $L/L_{\_FV}$ of 6, as shown in Figure 5. For a deflagration, the high pressure core is followed immediately by a negative phase over the range of flame speeds examined.

Flame acceleration and possible DDT

For an unconfined elongated VCE with a uniform fuel concentration and congestion patter, the initial rapid phase of flame acceleration occurs within the normalized distance (L/L_{FV}) region between 2 and 4. If a DDT does not occur, an approximately constant subsonic flame speed will then be reached within the normalized distance (L/L_{FV}) region between 4 and 6. The transition between the initial acceleration and constant flame speeds is mainly due to the initial spherical (and cylindrical, if applicable) expansion and the resultant turbulent burning. This flame behaviour was observed in both the BakerRisk and Buncefield JIP test rigs.

Referring to Figure 12, it can be seen that for a flame speed of Mach 0.9 attained within the normalized distance (L/L_{FV}) region between 2 and 4, the primary and secondary peaks have not decoupled in L/L_{FV} =4 and 6. As a result, any small positive-feedback disturbances in this region may trigger additional flame acceleration and result in a DDT. At a flame speed of Mach 0.6 (see Figure 11), the decoupling between the primary and secondary peaks is not significant in the normalized distance (L/L_{FV}) region between 4 and 6, and hence flames traveling at this speed would be most susceptible to a DDT in this range. Of course, the disturbance required for a Mach 0.6 flame to DDT would be much greater than with a Mach 0.9 flame.

Conclusions

For an unconfined elongated VCE with a uniform fuel concentration and congestion pattern, an initial rapid phase of flame acceleration occurs within the normalized distance (L/L_{FV}) region between 2 and 4. If a DDT does not occur, an approximately constant subsonic flame speed will be reached within the normalized distance (L/L_{FV}) region between 4 and 6. During the constant flame speed phase, an isolated high pressure core travels with the flame front, followed by a negative phase. The negative phase is generated by the primary blast wave developed during the initial acceleration phase.

For the case with a higher flame speed ($M_f > 0.6$), the blast wave outside the cloud/congestion experiences a significant pressure drop from the peak positive pressure to peak negative pressure within the normalized characteristic time (t_n). The magnitude of the pressure drop between the peak positive and negative pressures diminishes quickly with distance.

If a flame speed of Mach 0.9 is attained within a normalized distance (L/L_{FV}) of 2 and 4, the decoupling between the primary peak and the secondary peak beyond an L/L_{FV} of 4 is diminished. A DDT may occur if a positive-feedback disturbance (e.g., congestion pattern change) within the normalized distance range of 4 to 6 is present.

The blast wave shape within the elongated cloud and in the near-field exhibits a behaviour belonging to the acoustic wave regime no matter how high flame speed as long as the flame speed is less than unit (i.e., subsonic flame), while the magnitudes of the peak positive and negative phases are larger than with a traditional acoustic wave. Further study is required to investigate any blast wave shape difference in the mid- and far-field generated by the elongated VCEs and the traditional hemispherical VCEs.

References

Baker, W.E., Explosion in Air, University of Texas Press, Austin, TX, 1973.

Baker, W.E., Cox, P.A., Westine, P.S., Kulesz, J.J. and Strehlow, R.A., Explosion Hazards and Evaluation, Elsevier, 1983.

van den Berg, A.C., "The Multi-Energy Method - A Framework For Vapor Cloud Explosion Blast Prediction", *J. of Hazard Materials*, **12**, 1-10, 1985

Center for Chemical Process Safety, Guidelines for Vapor Cloud Explosion, Pressure Vessel Burst, BLEVE and Flash Fire Hazards, American Institute of Chemical Engineers, John Wiley & Sons, Hoboken, NJ, 2010.

Geng, J.H. and Thomas, J.K., "Simulation and Application of Blast Wave-Target Interaction," Proceedings of the 41st Annual Loss Prevention Symposium, Houston, Texas, 2007.

Geng, J.H, Thomas, J.K. and Baker, Q.A., "Pressure Vessel Burst Directional Blast Effects," Paper No. PVP2011-57167, ASME 2011 Pressure Vessels and Piping Conference, Baltimore, MD, July 17-21, 2011.

Geng, J.H, Mader, T. and Baker, Q.A., "Blast Wave Clearing Behavior for Positive and Negative Phases" J. of Loss Prevention in the Process Industries (2014), http://dx.doi.org/10.1016/j.jlp.2014.10.018

Lenoir, E.M., and Davenport, J.A., "A Survey of Vapor Cloud Explosions-Second Update", 26th Loss Prevention Symposium, AIChE, 1992

Pickles, J.H. and Bittleston, S,H., "Unconfined Valor Cloud Explosions – The Asymmetrical Blast from an Elongated Cloud", *COMBUSTION AND FLAME*, 51: 45-53, 1983

Strehlow, R.A., Luckritz, R.T., Adamczyk, A.A. and Shimp, S.A.,"The Blast Wave Generated By Spherical Flames", *COMBUSTION AND FLAME*, 35: 297-310, 1979

Thomas, J.K., M.L. Goodrich, J.N. Dyer, J. Geng and D.E. Ketchum (2006) "Petrochemical Plant Explosion Consequence Assessment," EASEC-10, East Asia-Pacific Conference on Structural Engineering and Construction, Bangkok, Thailand, August 3-5, 2006.

Tang, M.J. and Baker, Q.A., "A New Set of Blast Curves for Vapor Cloud Explosions," Center for Chemical Process Safety (CCPS)/AIChE, 33rd Loss Prevention Symposium, 1999.

van den Berg, A.C., "The Multi-Energy Method - A Framework For Vapor Cloud Explosion Blast Prediction", *J. of Hazard Materials*, **12**, 1-10, 1985